An Extended Ice-Age Sea-Level Equation: Incorporating Water Flux Across Sills

Sophie Coulson[1], David Al-Attar[2] and Jerry Mitrovica[1]

[1] *Department of Earth and Planetary Sciences, Harvard University, Cambridge, MA, USA.*

[2] *Bullard Laboratories, Department of Earth Sciences, University of Cambridge, Cambridge, UK.*

Corresponding Author: Sophie Coulson, slcoulson@g.harvard.edu

SUMMARY

We present a generalized theory governing gravitationally self-consistent, spatio-temporal sea-level changes within an ocean-plus-lake system that is intermittently connected by water mass flux across a sill. Our expressions for the change in sea level (defined as the difference in height of the sea surface equipotential relative to the solid surface) hold for any Earth model, and easily incorporate effects of viscoelastic deformation of the solid Earth and perturbations in both the gravitational field and rotation vector (as is now standard in ice-age sea-level calculations). In its most general form, the theory also includes an exact treatment of the evolving shoreline position in both water bodies. Our formalism involves three cases: (1) one global ocean, in which mass transfer may occur between ice sheets and the global ocean; (2) an ocean and lake separated by an exposed sill, in which mass transfer may occur between ice sheets and the global ocean, and between the ocean and lake via evaporative flux; and (3) transitional phases between these two states, when the ocean surface reaches the height of the sill from below (i.e., the sill is breached) or above (the sill is exposed). We illustrate the new theory using examples from the Black Sea flooding during the last deglacial phase ($\sim$10 ka) and sea-level fall in the Mediterranean Sea during the Messinian Salinity Crisis (5.96-5.33 Ma). These exam-

ples demonstrate the importance of including the geophysical feedbacks associated with sea-level change in an isolated basin in the dynamics of flooding and desiccation.

Key words: Sea level change, Loading of the Earth

1 INTRODUCTION

The theory governing gravitationally self-consistent ice-age sea-level changes has its roots in studies dating back more than a century (Woodward, 1888). The first modern treatment of the problem was given in the classic article of Farrell and Clark (1976), which calculated sea-level changes driven by ice mass flux on non-rotating, spherically symmetric Earth models, and in deriving their so-called "sea-level equation", it was assumed that geometry of shorelines was fixed in time. Under the assumption of 1-D (i.e., depth varying) Earth properties, the perturbation in sea level - formally defined as the vertical distance between the sea-surface equipotential and the solid surface - was expressed in terms of viscoelastic surface load Love numbers (Peltier, 1974). Spatial (Peltier and Andrews, 1976) and spectral (Mitrovica and Peltier, 1991) approaches were subsequently developed for solving the sea-level equation, although the pseudo-spectral algorithm described by Mitrovica and Peltier (1991) and later Kendall et al. (2005) has become the standard approach adopted in the ice-age sea-level community.

Beginning in the late 1980s, a series of articles extended the sea-level theory to account for the migration of shorelines associated with local onlap or offlap of water (Lambeck and Nakada, 1990; Milne et al., 1999; Johnston, 1993; Peltier and Drummond, 2002) and changes in the perimeter of grounded, marine-based ice (Milne et al., 1999). These studies applied various levels of approximation to account for these effects; an exact treatment of both, valid for Earth models of arbitrary complexity, was derived by Mitrovica and Milne (2003). More recent studies have begun to include the changing surface loads of water stored on land, particularly in pro-glacial lakes that develop during ice sheet retreat (Lambeck et al., 2017).

Changes in sea level associated with perturbations to Earth rotation have also been incorporated into the sea-level equation (Han et al., 1989; Milne and Mitrovica, 1996, 1998; Bills and James, 1996; Peltier, 1998; Mitrovica et al., 2005). There are two parts to any calculation of this effect: the perturbation to Earth rotation driven by ice-age surface mass changes and the impact of this perturbation on sea level. Mitrovica et al. (2005) demonstrated that earlier calculations of the former (e.g. Wu and Peltier, 1984) were characterized by a major inaccuracy associated with the treatment of the Earth's equatorial bulge, and they provided a revised theory that resolved this issue. Kendall et al. (2005) provided

algorithms for solving the generalized sea-level equation of Mitrovica and Milne (2003) appropriate for rotating Earth models of arbitrary complexity.

There is an important, underlying assumption in all the above treatments, namely, that any location where sea level is greater than zero - that is, where the solid surface lies below the sea-surface equipotential - will be subject to water mass changes as ice sheets grow and diminish, even if the location is not connected to the global ocean. For example, at present-day topography, low lying areas such as Death Valley and inland seas like the Caspian Sea, would experience water influx to the level of the evolving sea-surface equipotential if ice sheets melted. If such regions always remain disconnected from the global ocean, then a solution to this issue is straightforward: a mask can applied to the topography that excludes these as accommodation space for meltwater across the glacial cycle. However, this solution is not appropriate when a sill that connects the isolated water body to the ocean can be breached. In that case, the regions on both sides of the sill would be subject to the full suite of gravitational, deformation and rotational effects associated with surface mass load changes anywhere on the globe, but would evolve as separate entities until the breach occurred.

A notable example of this scenario would be in the Black Sea, where the rise in global sea level across the last deglacial phase led to a breach of the Bosphorus Sill and a connection of the sea to the global ocean at $\sim$10 ka (Ryan et al., 2003). Ice-age sea-level calculations of the flooding event have been performed (Lambeck et al., 2007; Goldberg et al., 2016); however, these studies adopted various approximations to the sea-level theory such that the resulting solutions were not gravitationally self-consistent. Other examples from the last deglacial phase include reflooding of the Caspian Sea (17-10 Ka) and the Persian Gulf (14-6 Ka)(Chepalyga, 2007; Teller et al., 2000; Lambeck, 1996). Evidence for flooding in previous deglacials has also been identified in the English Channel, indicating outburst flooding across the Dover Strait from a large meltwater lake (Gupta et al., 2007).

A complex situation occurred in the Mediterranean Sea during the Messinian Salinity Crisis from 5.96-5.33 Ma. During this period, the Mediterranean Sea was subject to numerous cycles of sea-level drawdown and inundation, followed by a longer phase of complete isolation and desiccation, which ended in a dramatic breaching of the Gibraltar and Sicily sills known as the Zanclean flood (e.g. Clauzon et al., 1996; Gargani and Rigollet, 2007; Rohling et al., 2008; Roveri et al., 2014; Garcia-Castellanos et al., 2009). The initial stage of cyclicity may have been a response to the competing effects of erosion and tectonic uplift of the sill (Garcia-Castellanos and Villaseñor, 2011), sea-level oscillations driven by variations in the size of the Antarctic Ice Sheet (Ohneiser et al., 2015), precessionally forced variations in local climate (Krijgsman et al., 1999, 2001; Lugli et al., 2010) or some combination of the three. An initial effort to apply ice-age sea-level theory to the cyclicity, based on an approximate treatment of the water loading signal within the Mediterranean Sea, demonstrated that ne-

glecting gravitational and deformational effects associated with sea-level change in the Mediterranean basins introduces significant inaccuracies in predictions of the magnitude and direction of sea-level change at the Gibraltar Strait (Coulson et al., 2019).

In this article, we extend the generalized sea-level theory of Mitrovica and Milne (2003) to derive a gravitationally self-consistent treatment of water redistribution in the case where a region characterized by positive sea level (i.e., where the crust sits below the local sea-surface equipotential) is subject to episodes of either connection or disconnection to the global ocean. The theory allows for perturbations in sill height associated with local sea-level changes and is valid for Earth models of arbitrary complexity. The theory also incorporates the possibility of evaporative mass transport across the sill, which is of particular importance for studying the Mediterranean basins, where evaporation rates dramatically exceed recharge rates. The next section outlines the extended sea-level theory. To best illustrate the capabilities of this novel approach, a subsequent section presents calculations for idealized lake-ocean systems, based on the Black Sea flooding and desiccation of the Mediterranean Sea.

2 THEORY

Our sea-level formalism will involve three cases: one global ocean, a two water body system involving an ocean and lake separated by an exposed sill, and transitional phases that occur between the single and double water body states. For simplicity, we begin with a system with no shoreline migration, that is, following the original assumption of Farrell and Clark (1976), we assume that shorelines are characterized by steep vertical cliffs. A full theoretical and numerical implementation that incorporates shoreline migration is given in Appendix A. In the following, we adopt the notation of Mitrovica and Milne (2003) and Kendall et al. (2005).

2.1 One Water Body

Global sea level is formally defined as the elevation difference between the height of the sea-surface equipotential (G) and the solid surface (R) (see Fig. 1):

$$SL(\theta, \psi, t) = G(\theta, \psi, t) - R(\theta, \psi, t), \tag{1}$$

where θ and ψ are colatitude and east longitude, respectively, and t is time. Sea level can be expressed as a perturbation, $\Delta SL(\theta, \psi, t)$, from an initial state at $t = t_0$,

$$SL(\theta, \psi, t) = SL(\theta, \psi, t_0) + \Delta SL(\theta, \psi, t) \tag{2}$$

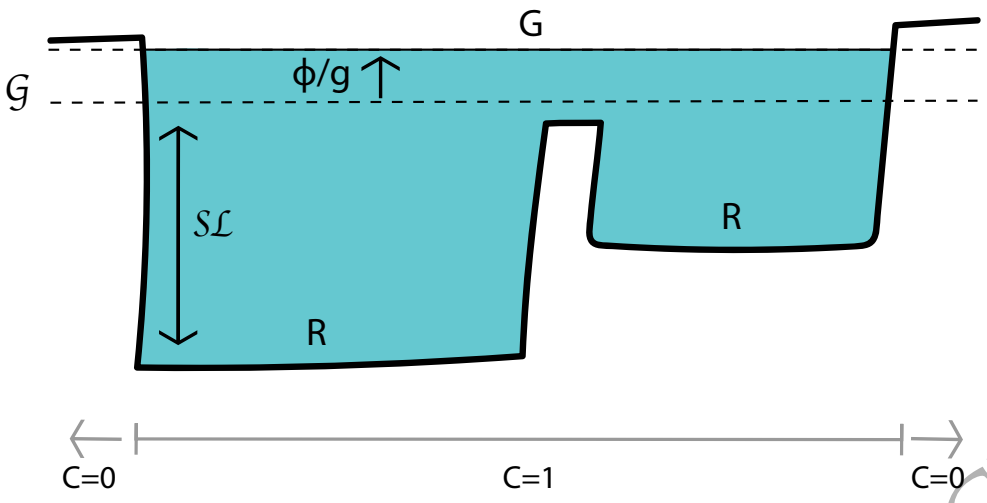

Figure 1. Schematic illustration of the global ocean system. The bounding surfaces G and R, components of sea level $\mathcal{SL}$, $\mathcal{G}$ and ϕ/g, and the ocean function C are defined in the text (see Equations 1, 7 and 8). We refer to these quantities both as totals, as perturbations from the initial state, Δ, and as changes across a single time step, δ.

where

$$\Delta SL(\theta,\psi,t) = \Delta G(\theta,\psi,t) - \Delta R(\theta,\psi,t). \tag{3}$$

In this system, topography is defined as the negative of sea level, i.e., the height of the solid surface relative to the elevation of the sea-surface equipotential:

$$T(\theta,\psi,t) = -SL(\theta,\psi,t) = T(\theta,\psi,t_0) + \Delta T(\theta,\psi,t) = T(\theta,\psi,t_0) - \Delta SL(\theta,\psi,t). \tag{4}$$

A simple expression relates changes in ocean height to changes in global sea level:

$$\Delta S(\theta,\psi,t) = \Delta SL(\theta,\psi,t) C(\theta,\psi), \tag{5}$$

where we have assumed that shoreline geometry is fixed in time. In this expression, $C(\theta,\psi)$ is the ocean function defined as:

$$C(\theta,\psi) = \begin{cases} 1 & \text{over oceans, i.e., where } SL(\theta,\psi,t) > 0 \\ 0 & \text{elsewhere.} \end{cases} \tag{6}$$

Following the ice-age literature, we next decompose $\Delta G(\theta,\psi,t)$ in Equation (3), and thus the sea-level change, $\Delta SL(\theta,\psi,t)$, into a geographically variable part and a uniform shift $\Delta\phi(t)/g$. In

particular,

$$\Delta SL(\theta,\psi,t) = \Delta\mathcal{SL}(\theta,\psi,t) + \frac{\Delta\phi(t)}{g}, \tag{7}$$

where

$$\Delta\mathcal{SL}(\theta,\psi,t) = \Delta\mathcal{G}(\theta,\psi,t) - \Delta R(\theta,\psi,t). \tag{8}$$

$\Delta\mathcal{G}$ represents the spatially variable component of the perturbation to the height of the sea-surface equipotential from its initial state. This decomposition recognizes that whilst the ocean surface must remain an equipotential surface in a static sea-level theory, the value of the equipotential can change in time. Using Equation (7), we can rewrite Equation (5) as

$$\Delta S(\theta,\psi,t) = \left[\Delta\mathcal{SL}(\theta,\psi,t) + \frac{\Delta\phi(t)}{g}\right] C(\theta,\psi). \tag{9}$$

$\Delta\mathcal{SL}$ is computed as a response to the total surface mass load change, ΔL, which can be decomposed into components associated with the water (ΔS) and ice (ΔI) load:

$$\Delta L(\theta,\psi,t) = \rho_w \Delta S(\theta,\psi,t) + \rho_i \Delta I(\theta,\psi,t) \tag{10}$$

where ρ_w and ρ_i are the densities of water and ice, respectively.

The uniform shift in the height of the sea-surface equipotential can be computed by invoking conservation of the surface mass load. Integrating both sides of Equation (9) over the surface of the Earth yields

$$\frac{\Delta\phi(t)}{g} = \frac{1}{A}\iint_\Omega \Delta S(\theta,\psi,t) - \frac{1}{A}\iint_\Omega \Delta\mathcal{SL}(\theta,\psi,t) C(\theta,\psi)\mathrm{d}\Omega, \tag{11}$$

where A is the area of the ocean

$$A = \iint_\Omega C(\theta,\psi)\mathrm{d}\Omega. \tag{12}$$

Next, conservation of the surface mass load requires that

$$\iint_\Omega \Delta S(\theta,\psi,t)\mathrm{d}\Omega = -\frac{\rho_i}{\rho_w}\iint_\Omega \Delta I(\theta,\psi,t)\mathrm{d}\Omega, \tag{13}$$

and using this expression in Equation (11) yields

$$\frac{\Delta\phi(t)}{g} = -\frac{1}{A}\frac{\rho_i}{\rho_w}\iint_\Omega \Delta I(\theta,\psi,t)\mathrm{d}\Omega - \frac{1}{A}\iint_\Omega \Delta\mathcal{SL}(\theta,\psi,t) C(\theta,\psi)\mathrm{d}\Omega. \tag{14}$$

Equations (6), (9) and (14) govern the redistribution of water associated with ice mass flux, i.e., the "sea-level equation" for the system.

In considering an ocean and lake system which are intermittently connected, it will be more convenient - both in the derivation below and in the numerical implementation - to proceed not by considering changes in sea level from the start of the simulation, but rather across each time step in the

simulation. A given simulation can include multiple switches from a one body to two body state, or vice versa, with transitions between the two states occurring across a single time step, and thus updates in the ocean load are more compactly expressed across individual time steps. Of course, a simple relationship exists between changes in the ocean load as expressed above and changes across a single time step. For example, for the j^{th} time step,

$$\Delta S(\theta, \psi, t_j) = \Delta S(\theta, \psi, t_{j-1}) + \delta S(\theta, \psi, t_j). \tag{15}$$

Similar expressions can be written for other time-dependent quantities, e.g., $\Delta\mathcal{SL}$, ΔI, and $\Delta\phi$. In this case, the sea-level equation for the j^{th} time step is:

$$\delta S(\theta, \psi, t_j) = \left[\delta\mathcal{SL}(\theta, \psi, t_j) + \frac{\delta\phi(t_j)}{g}\right] C(\theta, \psi), \tag{16}$$

where

$$\delta SL(\theta, \psi, t) = \delta\mathcal{SL}(\theta, \psi, t) + \frac{\delta\phi(t)}{g}, \tag{17}$$

and

$$\frac{\delta\phi(t_j)}{g} = -\frac{1}{A}\frac{\rho_i}{\rho_w}\iint_\Omega \delta I(\theta, \psi, t_j)\mathrm{d}\Omega - \frac{1}{A}\iint_\Omega \delta\mathcal{SL}(\theta, \psi, t_j)C(\theta, \psi)\mathrm{d}\Omega. \tag{18}$$

All of the above expressions are general and make no assumption in regard to the Earth model. We note that since the geographically variable component of sea-level change, $\Delta\mathcal{SL}(\theta, \psi, t)$ or $\delta\mathcal{SL}(\theta, \psi, t)$, is a function of the ocean load, Equations (9) and (16) are integral equations.

2.2 Two Isolated Water Bodies: Ocean & Lake

Next we consider the case of two isolated water bodies: a global ocean and lake separated by an exposed sill (Fig. 2). We use subscripts 'o' and 'm' to differentiate the two. The sea-level equation governing the redistribution of water in the global ocean is given by:

$$\delta S_o(\theta, \psi, t_j) = \left[\delta\mathcal{SL}(\theta, \psi, t_j) + \frac{\delta\phi_o(t_j)}{g}\right] C_o(\theta, \psi), \tag{19}$$

and the analogous expression governing the gravitationally self-consistent change in the water load within the lake is

$$\delta S_m(\theta, \psi, t_j) = \left[\delta\mathcal{SL}(\theta, \psi, t_j) + \frac{\delta\phi_m(t_j)}{g}\right] C_m(\theta, \psi). \tag{20}$$

The expressions for δS_o and δS_m are coupled through the geographically variable component of the change in global sea level, $\delta\mathcal{SL}$. This connection arises because the global sea-level change is driven by the total surface mass load; so, for example, the loading history in the lake will impact sea

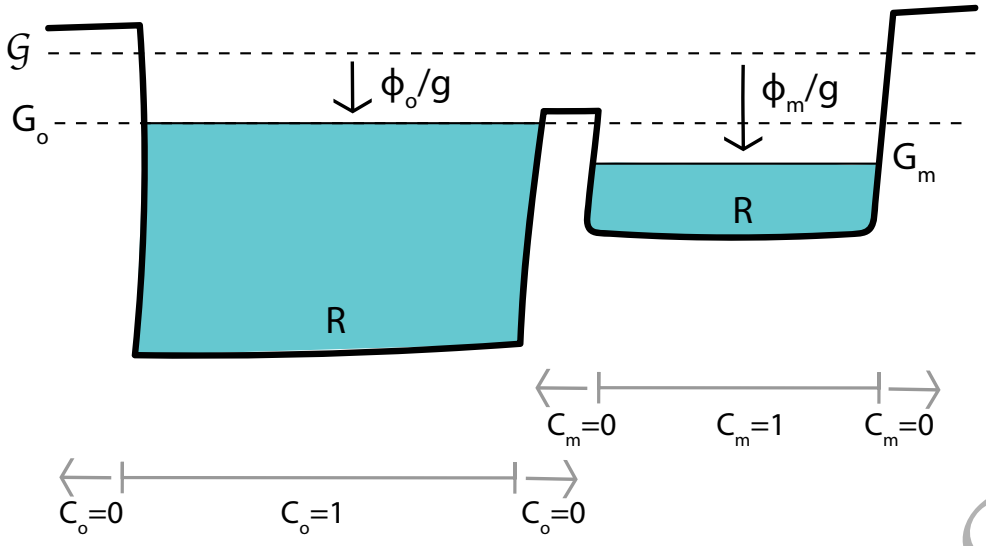

Figure 2. Schematic illustration of the isolated lake and ocean system. The larger basin on the left represent the global ocean, with the smaller basin on the right representing a disconnected lake. The bounding surfaces, components of sea level, and the ocean functions are defined in the text. We refer to these quantities both as totals, as perturbations from the initial state, Δ, and as changes across a single time step, δ.

level in the ocean, and vice versa. We note also that the sea-surface equipotential associated with the ocean represents the bounding surface of sea level throughout the globe (Fig. 2). The surface of the lake is also an equipotential, but if the lake is isolated from the ocean, the value of this equipotential is distinct from the ocean surface equipotential, and the difference in the two gravitational potentials is given by $\delta\phi_o(t) - \delta\phi_m(t)$.

From Equations (19) and (20), each of the water bodies has its own projection operator, which we may write as

$$C_o(\theta,\psi) = \begin{cases} 1 & \text{within ocean} \\ 0 & \text{elsewhere} \end{cases} \tag{21}$$

$$C_m(\theta,\psi) = \begin{cases} 1 & \text{within lake} \\ 0 & \text{elsewhere} \end{cases} \tag{22}$$

The change in the surface mass load across the time step is given by:

$$\delta L(\theta,\psi,t_j) = \rho_w[\delta S_o(\theta,\psi,t_j) + \delta S_m(\theta,\psi,t_j)] + \rho_i \delta I(\theta,\psi,t_j). \tag{23}$$

To derive expressions for $\delta\phi_o(t_j)$ and $\delta\phi_m(t_j)$, we integrate both sides of Equations (19) and (20),

respectively, over the surface of the Earth. For the open ocean this yields

$$\frac{\delta\phi_o(t_j)}{g}\iint_\Omega C_o(\theta,\psi)\mathrm{d}\Omega = \iint_\Omega \delta S_o(\theta,\psi,t_j) - \iint_\Omega \delta\mathcal{SL}(\theta,\psi,t_j)C_o(\theta,\psi)\mathrm{d}\Omega. \tag{24}$$

Assuming that the global reservoir of ice is in direct contact with the ocean not the lake, conservation of the surface mass load requires that

$$\iint_\Omega \delta S_o(\theta,\psi,t_j)\mathrm{d}\Omega = -\frac{\rho_i}{\rho_w}\iint_\Omega \delta I(\theta,\psi,t_j)\mathrm{d}\Omega + \delta E(t_j), \tag{25}$$

where the new term, $\delta E(t)$, represents the prescribed volume of water transferred from the lake to the open ocean during the time step by evaporation (the sign of the parameter will be negative if the net mass flux is from the ocean to the lake). Using Equation (25) in (24) and solving for $\delta\phi_o(t_j)/g$ yields

$$\frac{\delta\phi_o(t_j)}{g} = -\frac{1}{A_o}\frac{\rho_i}{\rho_w}\iint_\Omega \delta I(\theta,\psi,t_j)\mathrm{d}\Omega + \frac{\delta E(t_j)}{A_o} - \frac{1}{A_o}\iint_\Omega \delta\mathcal{SL}(\theta,\psi,t_j)C_o(\theta,\psi)\mathrm{d}\Omega, \tag{26}$$

where

$$A_o = \iint_\Omega C_o(\theta,\psi)\mathrm{d}\Omega. \tag{27}$$

The analogous expression for $\delta\phi_m(t_j)/g$ is:

$$\frac{\delta\phi_m(t_j)}{g} = -\frac{\delta E(t_j)}{A_m} - \frac{1}{A_m}\iint_\Omega \delta\mathcal{SL}(\theta,\psi,t_j)C_m(\theta,\psi)\mathrm{d}\Omega \tag{28}$$

where

$$A_m = \iint_\Omega C_m(\theta,\psi)\mathrm{d}\Omega. \tag{29}$$

The coupled Equations (19), (20), (26) and (28), together with Equations (21) and (22), now govern the redistribution of water associated with ice mass flux and evaporation from the lake to the open ocean. As above, these changes across individual timesteps can be summed to give changes since the start of the simulation (e.g. Equation 15).

As mentioned in Section 2.1, topography is defined as the negative of sea level (Equation 4), and it evolves as we solve for sea level at each timestep. In the two water bodies case, within the maximum lake extent, topography is calculated relative to the equipotential surface of the lake, i.e., a shoreline of the lake will have zero topography. Elsewhere, topography is calculated relative to the equipotential surface of the global ocean.

2.3 Transitional Phases

Whenever the global ocean surface at the location of the sill reaches the height of the sill, either from above or below, the system enters a transitional phase in that time step. In the following, we discuss the two cases, one in which the global ocean surface falls to the level of the sill in the single global ocean case (Section 2.3.1), and one in which it rises to the level of the sill in the two water body

case (Section 2.3.2). Note an additional transitional case exists where, in a two water body case, the lake surface overtops the sill on the lake side, but the global ocean surface is below the sill on the ocean side. This latter case may arise as a result of deformational, gravitational and rotational effects associated with the changing surface mass load, and it can be treated using the same framework as that described in Section 2.3.1 since the desired end state is also $T_m(\theta_s, \psi_s, t) = 0$. The workflow of the code, highlighting the various transitional phases, is given in Appendix B.

2.3.1 Falling Sea Level: Disconnecting the Lake and the Global Ocean

We begin by considering the scenario of a single water body (Fig. 1) with falling sea level (Fig. 3A). In this case, as soon as the sill becomes exposed, the simulation transitions to the case of an isolated ocean and lake system. However, once the sill is exposed, any further ice mass change will be sourced from or fluxed to the ocean.

Beginning with the expressions for a single water body, the exposure of the sill is predicted to have occurred following any time step t_j in which sea level at the sill, $T(\theta_s, \psi_s, t_j)$ (Equation 4), where θ_s and ψ_s are the colatitude and longitude of the sill, is predicted to be positive. The calculation for that time step must then be corrected; specifically, one must transfer sufficient water out of the ocean and into the lake such that the lake level is pinned at the elevation of the sill (Fig. 3B). In the following, we will use the symbol d to emphasize that we are dealing with a correction term at time t_j to a time step in the simulation that has already been taken (i.e., a time step from $t = t_{j-1}$ to $t = t_j$ using the equations governing a single water body).

The equations governing this correction during the transition are similar to those derived in Section 2.2, with the exception that the transfer of water from the ocean to the lake does not involve any additional ice mass flux. The equations governing the redistribution of water are:

$$dS_o(\theta, \psi, t_j) = \left[d\mathcal{SL}(\theta, \psi, t_j) + \frac{d\phi_o(t_j)}{g} \right] C_o(\theta, \psi), \tag{30}$$

$$dS_m(\theta, \psi, t_j) = \left[d\mathcal{SL}(\theta, \psi, t_j) + \frac{d\phi_m(t_j)}{g} \right] C_m(\theta, \psi). \tag{31}$$

The flux of mass across the sill can be accounted for by introducing a volume flux term, $\Lambda(t)$, into expressions analogous to Equations (26) and (28):

$$\frac{d\phi(t_j)}{g} = -\frac{\Lambda(t_j)}{A_o} + -\frac{1}{A_o} \iint_\Omega d\mathcal{SL}(\theta, \psi, t_j) C_o(\theta, \psi) \mathrm{d}\Omega \tag{32}$$

$$\frac{d\phi_m(t_j)}{g} = \frac{\Lambda(t_j)}{A_m} - \frac{1}{A_m} \iint_\Omega d\mathcal{SL}(\theta, \psi, t_j) C_m(\theta, \psi) \mathrm{d}\Omega. \tag{33}$$

The flux of water necessary to fill the lake to the level of the sill is not known *a-priori*, but it can be efficiently solved for iteratively. A reasonable first guess ($k = 1$) for the volume flux across the sill

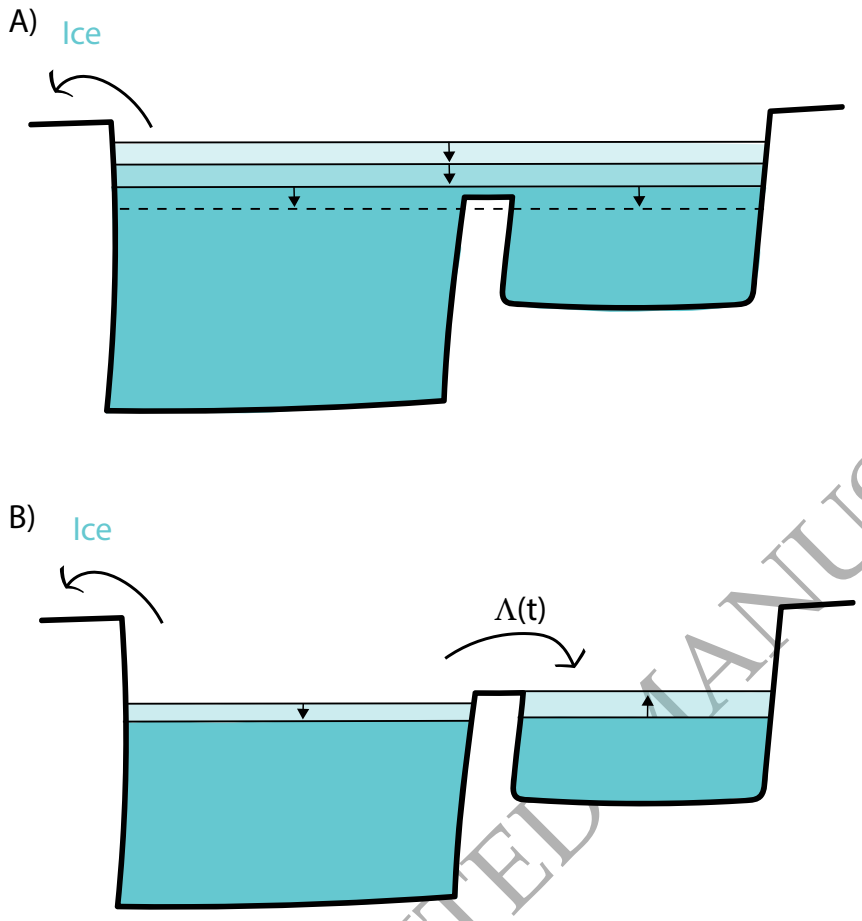

Figure 3. Schematic illustration of the transition from a global ocean to an isolated lake and ocean

would be the uniform amount that would fill the lake, transferred from the global ocean (as illustrated in Figure 3):

$$\Lambda(t_j)^{k=1} = T^*(\theta_s, \psi_s, t_j) \cdot A_m, \tag{34}$$

where $T^*(\theta_s, \psi_s, t_j)$ is the topography at the sill computed at $t = t_j$ for the one water body case, i.e., *before* any correction is applied to transfer water from the ocean to the lake. Successive improvements to this first guess for the volume flux across the sill are based on the computed topography on the lake

side of the sill, $T_m(\theta_s, \psi_s, t_j)$. Recalling that the change in topography is the negative of the change in sea level (e.g., Equation 4), sill topography during the iterative refinement can be written as:

$$T_o^k(\theta_s, \psi_s, t_j) = T^*(\theta_s, \psi_s, t_j) - \left[d\mathcal{SL}^k(\theta_s, \psi_s, t_j) + \frac{d\phi_o^k(t_j)}{g} \right], \tag{35}$$

$$T_m^k(\theta_s, \psi_s, t_j) = T^*(\theta_s, \psi_s, t_j) - \left[d\mathcal{SL}^k(\theta_s, \psi_s, t_j) + \frac{d\phi_m^k(t_j)}{g} \right]. \tag{36}$$

Whenever $T_m^k(\theta_s, \psi_s, t_j)$ is positive, more water must be transferred from the ocean to the lake, whereas if it is negative, the transfer is from lake to ocean. Accordingly, we can write

$$\Lambda(t_j)^{k+1} = \Lambda(t_j)^k + T_m^k(\theta_s, \psi_s, t) \cdot A_m, \tag{37}$$

and the process is repeated until the system of equations yields $T_m^k(\theta_s, \psi_s, t) = 0$ to within a specified tolerance.

After convergence ($k = \infty$), the total shift in water heights during the time step t_j of the simulation, required for the next time step, is given by:

$$\delta S_o(\theta, \psi, t_j) = \delta S^*(\theta, \psi, t_j) + dS_o^{k=\infty}(\theta, \psi, t) \tag{38}$$

$$\delta S_m(\theta, \psi, t_j) = \delta S^*(\theta, \psi, t_j) + dS_m^{k=\infty}(\theta, \psi, t) \tag{39}$$

We emphasize that at the end of the time step ($t = t_j$), the system is in a two body state, and one moves to the next time step using the equations described in Section 2.2.

2.3.2 Rising Sea Level: Connecting the Lake to the Global Ocean

Next, we consider the case of an initially isolated lake and ocean (Fig. 2), in which rising sea level in the global ocean, local to the sill, leads to a breach of the sill (Fig. 4A). In the time-varying evolution of the isolated ocean and lake simulation, if at any time step the topography on the ocean side of the sill, $T_o(\theta_s, \psi_s, t)$ changes sign from positive to negative, then water fluxes from the ocean to the lake. In this case, one of two scenarios will occur: (1) if the volume of excess water in the open ocean is sufficient to raise the lake level above the sill, the system will evolve into a one body state (Fig. 4C) and a single gravitational equipotential will define the water surface; (2) if the volume of excess water in the open ocean is not sufficient to fill the lake to the level of the sill, a flux of water from ocean to lake will occur until the ocean surface reaches the same height as the the sill, i.e., $T_o(\theta_s, \psi_s, t) = 0$ (Fig. 4B).

As in the first transitional state, above, the volume flux across the sill is not known *a-priori* but can be efficiently solved for iteratively. In both of the cases discussed in the preceeding paragraph,

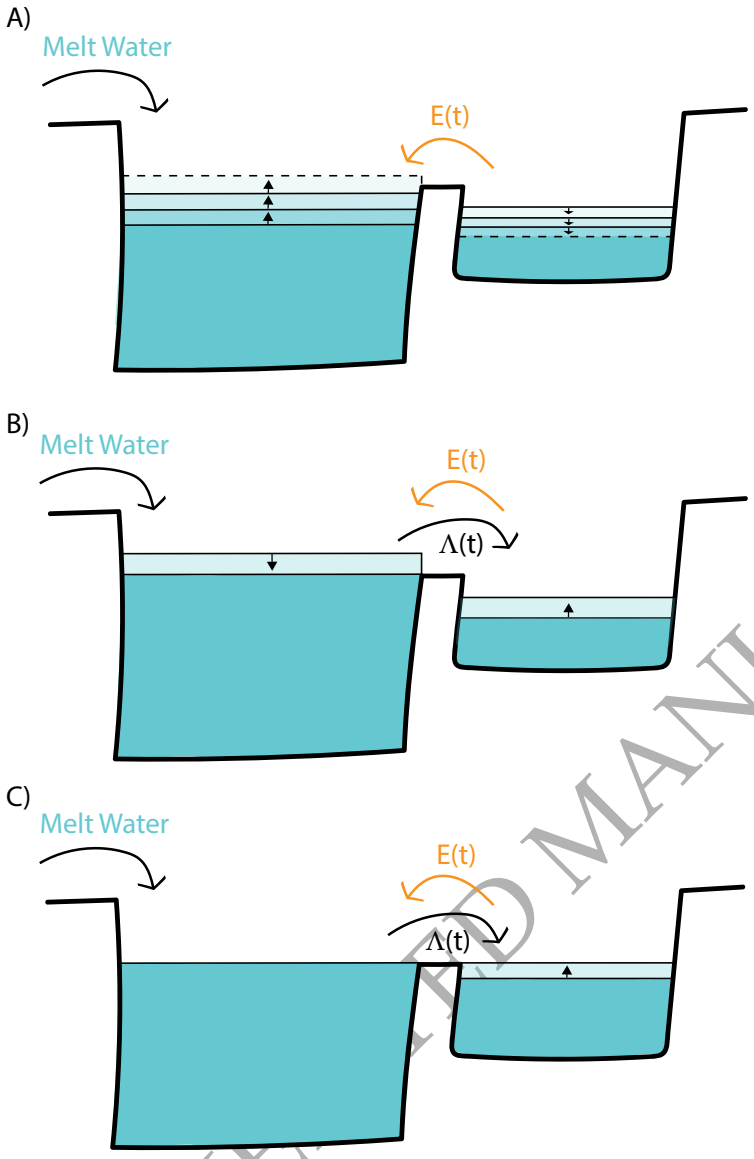

Figure 4. Schematic illustration of the transition from an isolated lake and ocean to a global ocean

the scheme defined by Equations (30) to (33) in Section 2.3.1, can be applied, but the scheme for iteratively improving a guess for the volume flux across the sill, $\Lambda(t)$, will be revised. Let us begin with the first case.

If the volume of excess water in the open ocean is large enough to raise the surface of the lake above the sill, a reasonable first guess for the volume flux across the time step would be:

$$\Lambda(t_j)^{k=1} = -\frac{[T_o^*(\theta_s, \psi_s, t_j) - T_m^*(\theta_s, \psi_s, t_j)] \cdot A_o}{A} \cdot A_m \tag{40}$$

where, the asterisk now denotes a topography computed at the time step $t = t_j$ under the assumption that the system was in a two body state before a correction is applied to transfer water from the ocean to lake. Physically, one is taking a uniform layer of thickness equal to the difference in height of the ocean and lake surfaces at the sill, $(T_o^*(\theta_s, \psi_s, t_j) - T_m^*(\theta_s, \psi_s, t_j))$, and distributing it equally across all of the new ocean area ($A = A_o + A_m$). As in Section 2.3.1, if this value was too high (i.e., the sea surface height in the lake becomes higher than that in the open ocean, or $T_m(\theta_s, \psi_s, t)$ is more negative than $T_o(\theta_s, \psi_s, t)$), water should be transferred from the lake to the ocean, and if it was too low, more water should be transferred from ocean to lake. The second iterate for $\Lambda(t)$ therefore takes the form:

$$\Lambda(t_j)^{k+1} = \Lambda(t_j)^k - \frac{[T_o^k(\theta_s, \psi_s, t_j) - T_m^k(\theta_s, \psi_s, t_j)] \cdot A_o}{A} \cdot A_m \tag{41}$$

The process is repeated until the topography on both sides of the sill become equal to within some tolerance, i.e., $T_m(\theta_s, \psi_s, t) \approx T_o(\theta_s, \psi_s, t)$. Inherent to the formulation, once this convergence is achieved the sea surface equipotentials of the lake and ocean also become equal ($\frac{\phi_o}{g} \approx \frac{\phi_m}{g}$). At convergence, one moves to the next time step in the sea-level theory using the equations governing the single global ocean, described in Section 2.1.

If the volume of excess water in the open ocean is not large enough to fill the water deficit in the lake, a reasonable first guess for the volume flux across the time step would be simply the volume of excess water

$$\Lambda(t_j)^{k=1} = -T_o^*(\theta_s, \psi_s, t_j) \cdot A_o, \tag{42}$$

with subsequent guesses following the form:

$$\Lambda(t_j)^{k+1} = \Lambda(t_j)^k - T_o^k(\theta_s, \psi_s, t_j) \cdot A_o. \tag{43}$$

Convergence is reached when the ocean surface reaches the sill height within some level of tolerance, i.e., $T_o(\theta_s, \psi_s, t) \approx 0$.

This transfer of mass in the correction procedure will generally act as a net load on the sill, since the rise in the height of the lake will be of greater magnitude than the drop in the level of the ocean, and the mass flux to the lake will also gravitationally attract water toward the sill. Both effects will lead to an increase in height of the ocean surface relative to the sill and a further, incremental breach of the sill. It is therefore to be expected that the incremental volume flux from ocean to lake will be positive in each iterative step.

After convergence of the iterative system of Equations (30)-(33), the total shift in water heights

during the time step t_j of the simulation, required for the next time step, is given by Equations (38)-(39). We emphasize that at $t = t_j$, the system is in a two body state.

3 SOME COMMENTS ON APPLYING THE NEW THEORY

The derivations above, and the more comprehensive ones that include shoreline migration in Appendix A, implicitly assume that a method exists for computing the geographically variable sea-level change, $\Delta\mathcal{SL}(\theta, \psi, t)$ or $\delta\mathcal{SL}(\theta, \psi, t)$, driven by arbitrary changes in the surface mass loading. In the case of 1-D linear viscoelastic Earth models, viscoelastic Love number theory (Peltier, 1974) can be used to derive expressions for these fields; we direct the reader to Kendall et al. (2005) for expressions that incorporate deformation, gravitational and rotational effects on sea level. For more complex Earth models and rheology, numerical schemes must be adopted to solve for them (e.g. Wu and van der Wal, 2003; Zhong et al., 2003; Latychev et al., 2005).

4 ILLUSTRATIVE EXAMPLES FOR IDEALIZED OCEAN-LAKE SYSTEMS

In this section we illustrate the flexibility of the new sea-level theory with idealized examples taken from the flooding history of the Mediterranean and the Black Seas. The simulations adopt a 1-D viscoelastic Earth model characterized by an elastic lithosphere of thickness 120 km, an upper mantle viscosity of 5×10^{20} Pa s, and a lower mantle viscosity of 5×10^{21} Pa s. Although all the predictions below include rotational effects on sea level, the physics at the sill is dominated by deformational and gravitational effects and thus we focus on the latter in the discussion below.

The complex network of basins in the Mediterranean region, combined with its diverse sea-level history provide an ideal setting in which to apply the sea-level theory described above. In addition to experiencing sea-level fluctuations due to the ice-age cycles of the Plio-Pleistocene, the Mediterranean region has also experienced sea-level fall due to its uniquely high evaporation rate. The evaporation rate exceeds precipitation and recharge, generating conditions which have led to the disconnection of seas in different basins and protracted periods of isolation from the open ocean.

The most remarkable example of limited connectivity between the Mediterranean Sea and the global ocean occurred during the Messinian Salinity Crisis (MSC, 5.96 Ma). The events of the MSC can be separated into two chronologically distinct stages (Clauzon et al., 1996). The first stage consisted of low amplitude fluctuations in Mediterranean sea level, which have been attributed to a variety of processes, including precessionally forced variations in local climate (Krijgsman et al., 1999, 2001; Lugli et al., 2010), the interplay between tectonic uplift and erosion at the Gibraltar sill (Garcia-Castellanos and Villaseñor, 2011), and variations in global sea level (Ohneiser et al., 2015). In the

second stage of the MSC, the Mediterannean was completely disconnected from the Atlantic Ocean and experienced a significant sea-level fall (Bache et al., 2015; Clauzon et al., 1996; Krijgsman et al., 1999), followed by dramatic reflooding of the Mediterranean basins, known as the Zanclean flood (Garcia-Castellanos et al., 2009; Periáñez and Abril, 2015).

Given the considerable controversy and uncertainty associated with both the timing and magnitude of each of these events, as a simple first example, we apply the new sea-level framework to consider a sinusoidal fluctuation in global sea level of magnitude 100 m driven by far field ice mass changes acting on modern day topography (Fig. 5). A sea-level fall of this magnitude is sufficient to expose the sill at the Gibraltar seaway (set to an initial depth of 60 m), thus isolating the Mediterranean 'lake' and pushing the system into a two water body state. Once the Mediterranean Sea has become isolated, it is subject to evaporative flux, representing the combined effect of evaporation, river run-off and precipitation. Here we choose a value of 0.4 m/yr for evaporative flux, in line with estimates for the Messinian period (Gladstone et al., 2007). As sea level in the open ocean rises again to the level of the Gibraltar sill, the sill is overtopped in a catastrophic flood and the system transitions back to the one water body state.

Fig. 6 shows the evolution of topography at several snapshots in time. When the system is in a two body state, topography within the maximum extent of the Mediterranean 'lake' is calculated relative to local sea surface height in the Mediterranean, as described in Section 2.2 (this is highlighted in Fig. 6B, with maximum 'lake' extent outlined in black and zero 'lake' topography highlighted in red). In the first 2300 years of the model run, while in the one water body state, the whole system evolves together with one global sea surface equipotential (Figs. 5 and 6A). After the Mediterranean has become isolated, we see a significant sea-level fall in the lake due to evaporative flux, shown in Figs. 5B and 6B. During this period, the system experiences gravitational and deformational changes in sea level associated with both the flux of water from the global ocean to the ice sheets, and from Mediterranean evaporation to the global ocean. The latter dominates the sea-level physics at the sill. That is, as water is removed from the Mediterranean basin, the crust at the sill will rebound due to the reduction in local surface mass loading, and the sea surface height of the sill will drop due to the reduction in the gravitational attraction exerted by the Mediterranean water load on the global ocean. These effects will combine to further expose the Gibraltar sill, prolonging the period of isolation, and increasing the total sea-level fall. In this scenario, the peak sea-level fall in the Mediterranean reaches $\sim$2100 m over the 6000 year period of isolation (Fig. 6B). Interestingly, at the peak sea-level fall, the Mediterranean 'lake' is split into two water bodies by the Sicily Sill becoming exposed. Our present formulation treats these two bodies as one, but could, in principle, be extended to incorporate a larger

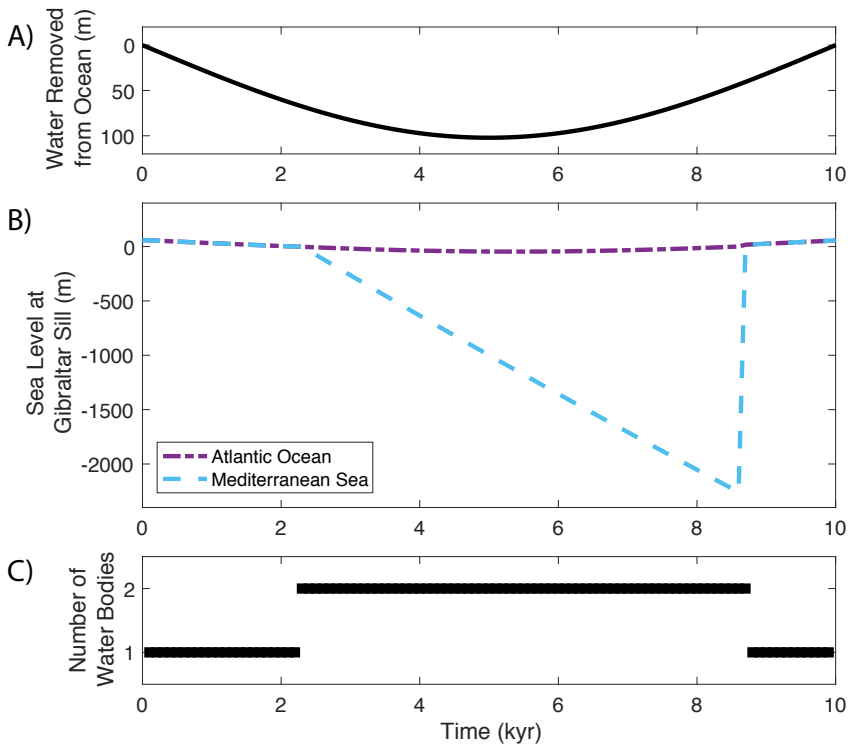

Figure 5. Sea level at the Gibraltar sill for a sinusoidal fluctuation in global sea level of 100 m. a) Global mean average height of water removed from the global ocean through time. b) Sea level on both the Atlantic Ocean side and the Mediterranean Sea side of the Gibraltar sill. c) Number of isolated water bodies present in the system.

number of water bodies to more accurately predict sea-level change in the individual Eastern and Western Mediterranean basins.

At the 5000 year point of the simulation, ice begins to melt and water starts to flux back into the ocean (Fig. 5A), and flooding of the Mediterranean begins ∼3400 years later (Figs. 5B, 6C). During the flooding stage, the physics described above reverses: as water moves across the sill from the open ocean to the Mediterranean Sea, the increased local mass load acts to depress the crust at the sill and its gravitational pull raises the height of the sea surface equipotential in the same area. Both of these effects increase sea level (lower topography) at the sill, producing a positive feedback, and leading to a run-away flood that occurs within one (100 yr) timestep of the simulation. A detailed view of the evolution of topography of the region through time is provided in Video 1 in the supplementary material.

A more recent example of dramatic sea-level change in the Mediterranean region occurred during the reflooding of the Black Sea during the last deglaciation phase of the ice age. At the Last Glacial

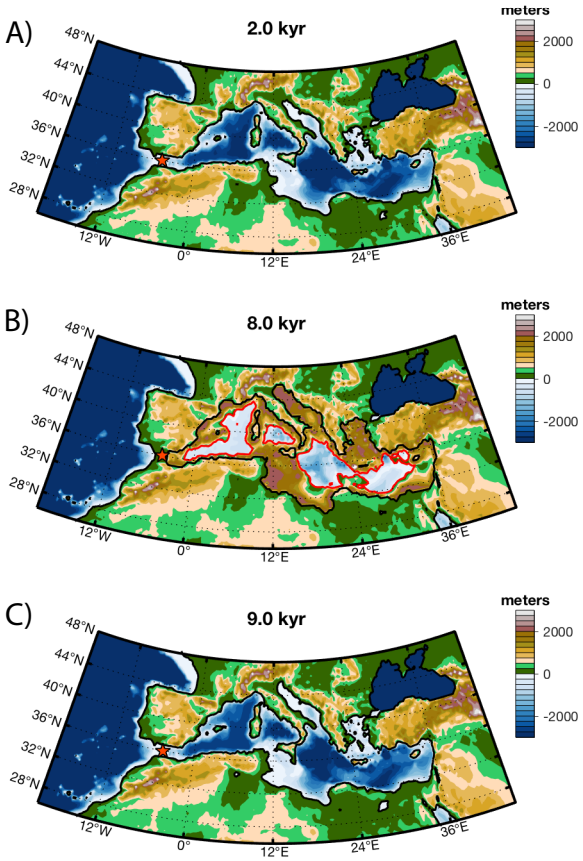

Figure 6. Evolution of topography for a sinusoidal fluctuation in global mean sea level of 100 m. Topography is shown a) 2000 years, b) 8000 years and c) 9000 years from the start of the simulation. The red star provides the location of the Gibraltar sill. Zero topography is highlighted in black while the Mediterranean Sea is connected to the global ocean, and in black and red for the global ocean and Mediterranean Sea, respectively, when the two water bodies are isolated from one another. While the two water bodies are isolated, the maximum extent of the Mediterranean lake is outlined in black. Note, the Black Sea is masked out for the purpose of this illustration.

Maximum (LGM), 26 ka, local sea level was significantly below the Marmara and Bosphorus Straits, breaking the connection between the Black Sea and the global ocean, and transforming the Black Sea into a freshwater or brackish lake fed by rivers and glacial melt water (Yanko-Hombach et al., 2014). As the ice sheets retreated and water rose in the Mediterranean, eventually the sills were breached, leading to an inflow of seawater into the Black Sea basin.

Despite significant stratigraphic and palaeontological evidence associated with this flooding event, the nature of Black Sea flood remains uncertain. The magnitude of the flood is primarily controlled by the pre-flood water height in the Black Sea basin, and estimates range from $\sim$ 100 m below present sea level (Ryan et al., 2003; Lericolais et al., 2010; Nicholas et al., 2011) to only 30-40 m below present sea level (Yanko-Hombach et al., 2014; Giosan et al., 2009). In contrast, rather than a catastrophic flooding

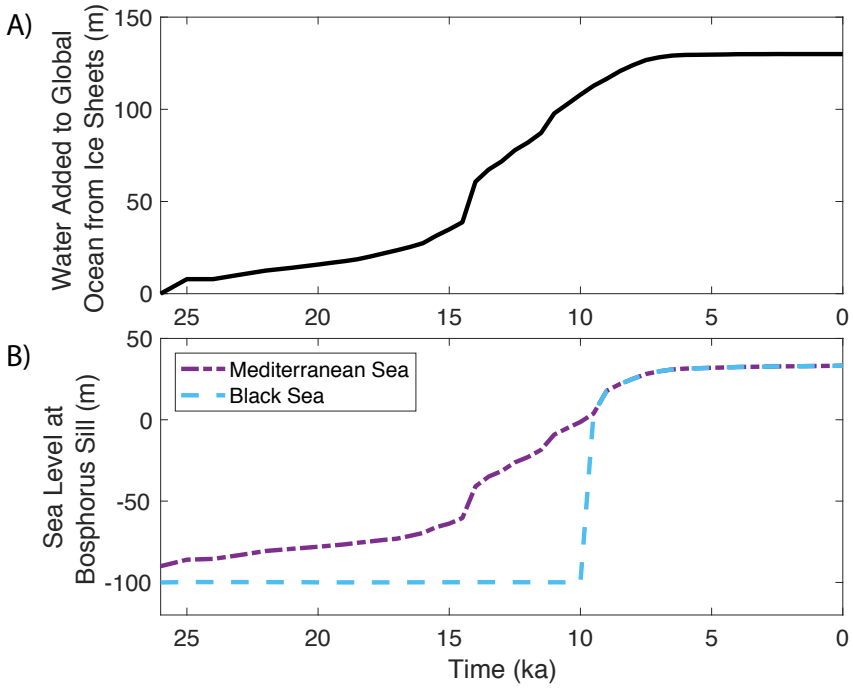

Figure 7. Sea level at the Bosphorus sill for ice sheet retreat beginning at 26 ka, as prescribed by the ICE-6G-C model (Peltier et al., 2015), and beginning with an isolated Black Sea basin. a) Global mean sea level rise through time. b) Sea level on both the Mediterranean Sea and Black Sea sides of the Bosphorus sill.

event, some studies argue that the reconnection between the two water bodies was characterized by a more gradual influx of water to the Black Sea (e.g. Aksu et al., 2002a). This theory is supported by seismic profiles and paleotonological data that suggest continual outflow from Black Sea to the Mediterranean Sea (Aksu et al., 2002b; Ferguson et al., 2018; Hiscott et al., 2002), implying that the surface of the Black Sea remained at, or close to, the elevation of the sill. The timing of reconnection is also controversial. Based on evidence from stratigraphy and various paleontological proxies from sediment cores, the flooding event has been dated from 12.8-7.1 Ka (Ryan et al., 1997; Major et al., 2002; Soulet et al., 2011; Yanko-Hombach et al., 2014). Geophysical modeling efforts are unable to reduce this range given uncertainties in both the height of the sill during the flood event and the pre-flood height of the isolated Black Sea (Goldberg et al., 2016).

Here we simulate a maximum flooding scenario for the Black Sea summarized in Fig. 7. From LGM to present, global mean sea level rose $\sim$130 m. The Bosphorus sill at LGM is prescribed to be 90 m above the surface of the Mediterannean Sea and 100 m above the level of the Black Sea. From this time to the present-day, our ice sheet history adopts the ICE-6G-C model (Peltier et al., 2015). The

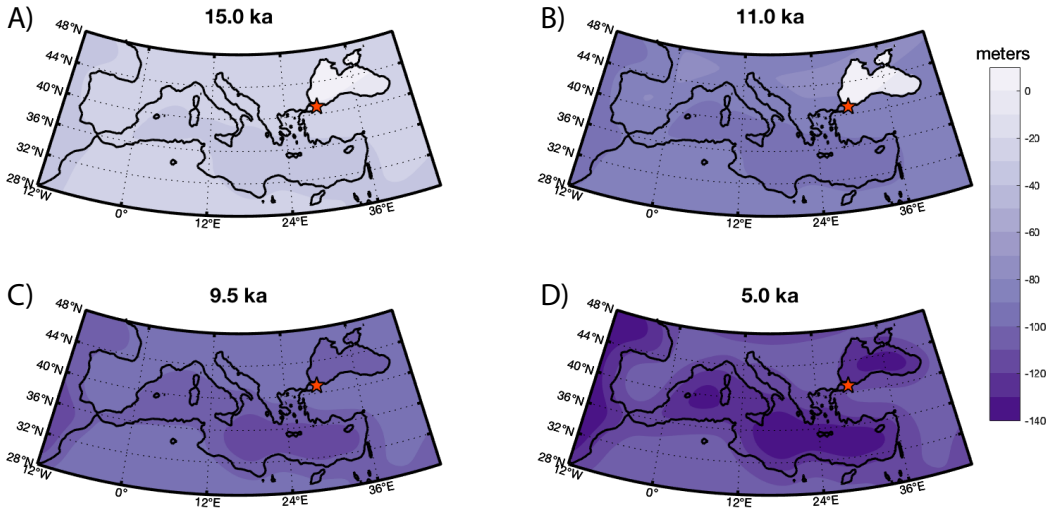

Figure 8. Computed change in topography relative to the start of the simulation, driven by ice sheet retreat and associated sea-level change since the Last Glacial Maximum. Snapshots show topography change a) at 15 ka, b) 11 ka, c) 9.5 ka and d) 5 ka. The red star gives the coordinates defining the Bosphorus sill. Zero initial topography is highlighted in black.

change in topography in the region relative to the start of the simulation for time slices encompassing the flood event in Fig. 8.

From 26 to 10 ka, the model is in a two water body state with evaporative flux set to zero. Thus, there is no water flux between the Black Sea and the global ocean, and the predicted (geographically variable) change in topography in Fig. 8A and B is simply the result of water moving from ice sheets into the global ocean, and the deformational and gravitational effects associated with this load change. At 9.5 ka, the sea surface on the Mediterranean side of the Bosphorus sill rises above the sill height, so water begins to overtop the sill. In this transitional phase the Black Sea floods, that is, topography subsides as the system evolves into a one water body state with a single sea-surface equipotential. At this stage, the simulation captures the sea-level change associated with both the melting of ice, and water flux into the Black Sea basin. The latter drives deformational and gravitational effects that act as a positive feedback on flooding, and the inundation of the Black Sea is completed within one time step of the simulation (Fig. 8C). Beyond this time, continued melting, water flux into both the Mediterranean and Black Sea, and ongoing isostatic adjustments drive further changes in the topography. A detailed view of how topography evolves through the duration of this model is given in Video 2 in the supplementary material.

To quantify the improvement in predictions generated using the theoretical treatment described above relative to previous studies, we compare results for a simplified flooding scenario for the

Mediterranean Sea (Figures 5, 6B and C) to the approximation in Coulson et al. (2019), based on applying the original sea-level theory of Mitrovica and Milne (2003). Figure C.1 shows various sea level predictions at the Gibraltar Sill through time for a scenario in which ice melting in the global ocean raises the sea surface 5 cm above the sill, thus initiating flooding. The solid black line on the figure represents the result of applying the new, extended sea level theory described in this article. This application ultimately leads to a complete filling of the Mediterranean ocean basin. The Coulson et al. (2019) treatment requires a predetermined flood volume and geometry. Specifically, a volume of water equal to the excess volume overtopping the sill in the global ocean is transferred as a uniform layer into the Mediterranean and no further flooding, or redistribution of flood water, is considered. In this case, adopting the approximation leads to a gross underestimation of the volume of water entering the Mediterranean Sea relative to the new theory and a prediction of only minor sea-level rise at the Gibraltar sill (red dash-dot line in Figure C.1). In an effort to improve the accuracy of this approximate treatment, we once again prescribe the volume and geometry of the flood, but using insight gained from our extended theory, we assume a water load precisely equal to the volume and geometry of the initial (unflooded) Mediterranean (shown in dashed blue). Once again, no redistribution of floodwater or further flooding is considered. This yields a prediction with an error of order 10% at the Gibraltar Sill. This error arises due to the neglect of both the additional volume of water that flows into the Mediterranean ocean basin, and the redistribution of water in the Mediterranean as the crust deforms and the sea surface equipotential evolves; both processes are captured using the new, gravitationally self-consistent treatment. We have also performed tests for the case of an emptying Mediterranean Sea with an evaporation rate of 4 m/yr, comparing removal of water according to the changing gravitational equipotential (in the extend theory) with removal of uniform sheets of water defined by the initial bathymetry of the Mediterranean Sea (Coulson et al., 2019). This yields inaccuracies on order of 10% at the Gibraltar sill from the beginning of the simulation. In both Coulson et al. (2019) and Goldberg et al. (2016), volume changes due to sill breach and/or evaporation, as well as their timing, are treated as known a priori, and volume changes are relatively small, thus these errors are mitigated.

5 FINAL REMARKS

The importance of including isostatic adjustment and gravitational effects associated with water redistribution to and from isolated basins in calculations of local sea-level change has been demonstrated in the literature, particularly in the Mediterranean region. Govers (2009) and Govers et al. (2009), for example, estimated the uplift associated with a large sea-level fall in the Mediterranean Sea, while Coulson et al. (2019) extended this to also include gravitational effects associated with mass flux in and

out of the Mediterranean Sea and focused on quantifying the impact of these effects on the dynamics of the Gibraltar sill. Lambeck et al. (2007) and Goldberg et al. (2016) used ice-age sea-level models to explore the timing and location of sill breach in the Black Sea flood, but neither study included a fully gravitationally self-consistent treatment of the flood event. Clark et al. (1990) predict uplift across the Great Lakes during the last deglaciation. To do so, they track individual elevation curves for potential lake outlets and calculate the location of the lowest ice-free outlet to infer drainage history. Their approach used a simplified sea-level model and does not account for load changes generated by water flowing through and out of the lake system. Clark et al. (2007) and Lambeck et al. (2017) developed algorithms to deal with scenarios in which water draining from an ice sheet enters a pro-glacial lake on land (or on ice), rather than immediately draining to the global ocean. Their methods ensure conservation of the surface mass load, but do not separately track the varying gravitational equipotential for each lake.

We provide the first complete gravitationally self-consistent sea-level theory that incorporates mass transfer both between ice sheets and the global ocean, and the global ocean and an intermittently disconnected and connected lake. Our framework extends the generalized sea-level theory of Mitrovica and Milne (2003) to capture the evolution of a one body (global ocean) system, a two body (ocean-plus-lake) system, and transitions in both directions between these two end states. The theory allows all deformational, gravitational and rotational effects of the surface mass loading of an arbitrary viscoelastic planet to be accounted for via a term describing change in sea level over time. For 1-D viscoelastic Earth models, this term can be expressed and computed using Love number theory, while for more complex Earth models a range of higher level computational methods have been developed in the ice-age sea-level literature to calculate it. The sea-level equations we have derived also account for evaporative mass transport across the sill during periods when the system is in a two water body state. The timing of the flooding of the lake, or its isolation from the open ocean, are governed entirely by the evolving system - the timing of these events is not prescribed. That is, once initial topographies, Earth model, ice history and evaporative transport are prescribed, these events occur when the evolving system predicts that the ocean surface reaches the sill height from below or above, respectively.

In a final section we present calculations for idealized ocean-lake systems that demonstrate the importance of including geographically variable sea-level changes in the filling or emptying of an isolated basin, particularly at the location of the sill (see also Coulson et al. (2019)). In these scenarios, geophysical processes associated with sea-level fall within an isolated basin act as a positive feedback, reducing sea level further at the sill and extending the period of isolation. The same is true in the case of sill overtopping and lake flooding: in this case, positive feedbacks act to escalate flooding. In fact, in both the Black Sea and Mediterranean test cases, we found that once flooding begins, the positive

feedbacks associated with crustal subsidence and increased gravitational attraction toward the lake lead to complete basin refilling within one time step of the simulations. These results indicate that the time scale of flooding will, in many cases, be limited only by the efficiency of water flux across the sill, rather than by water availability.

ACKNOWLEDGMENTS

We acknowledge MEDSALT (Uncovering the Mediterranean salt giant) COST Action CA15103 for useful discussion at the 2020 Final Symposium.We thank our two anonymous reviewers for constructive reviews that improved the final manuscript. S.C. is supported by Frank Knox Memorial Fellowships and Harvard University.

The code developed for this study can be obtained by contacting Sophie Coulson (slcoulson@g.harvard.edu).

References

Aksu, A., Hiscott, R., Yaşar, D., Işler, F., and Marsh, S. (2002a). Seismic stratigraphy of late quaternary deposits from the southwestern black sea shelf: evidence for non-catastrophic variations in sea-level during the last 10 000 yr. *Marine Geology*, 190(1-2):61–94.

Aksu, A. E., Hiscott, R. N., Kaminski, M. A., Mudie, P. J., Gillespie, H., Abrajano, T., and Yaşar, D. (2002b). Last glacial–holocene paleoceanography of the black sea and marmara sea: stable isotopic, foraminiferal and coccolith evidence. *Marine Geology*, 190(1-2):119–149.

Bache, F., Gargani, J., Suc, J.-P., Gorini, C., Rabineau, M., Popescu, S.-M., Leroux, E., Do Couto, D., Jouannic, G., Rubino, J.-L., et al. (2015). Messinian evaporite deposition during sea level rise in the gulf of lions (western mediterranean). *Marine and Petroleum Geology*, 66:262–277.

Bills, B. G. and James, T. S. (1996). Late quaternary variations in relative sea level due to glacial cycle polar wander. *Geophysical Research Letters*, 23(21):3023–3026.

Chepalyga, A. L. (2007). The late glacial great flood in the ponto-caspian basin. In *The Black Sea Flood Question: Changes in Coastline, Climate, and Human Settlement*, pages 119–148. Springer.

Clark, J. A., Pranger, H. S., Walsh, J. K., and Primus, J. A. (1990). A numerical model of glacial isostasy in the lake michigan basin. *Late quaternary history of the Lake Michigan Basin*, 251:111–123.

Clark, J. A., Zylstra, D. J., and Befus, K. M. (2007). Effects of great lakes water loading upon glacial isostatic adjustment and lake history. *Journal of Great Lakes Research*, 33(3):627–641.

Clauzon, G., Suc, J.-P., Gautier, F., Berger, A., and Loutre, M.-F. (1996). Alternate interpretation of the messinian salinity crisis: Controversy resolved? *Geology*, 24(4):363–366.

Coulson, S., Pico, T., Austermann, J., Powell, E., Moucha, R., and Mitrovica, J. X. (2019). The role of isostatic adjustment and gravitational effects on the dynamics of the messinian salinity crisis. *Earth and Planetary Science Letters*, 525:115760.

Farrell, W. and Clark, J. A. (1976). On postglacial sea level. *Geophysical Journal International*, 46(3):647–667.

Ferguson, S., Warny, S., Escarguel, G., and Mudie, P. J. (2018). Mis 5–1 dinoflagellate cyst analyses and morphometric evaluation of galeacysta etrusca and spiniferites cruciformis in southwestern black sea. *Quaternary International*, 465:117–129.

Garcia-Castellanos, D., Estrada, F., Jiménez-Munt, I., Gorini, C., Fernández, M., Vergés, J., and De Vicente, R. (2009). Catastrophic flood of the mediterranean after the messinian salinity crisis. *Nature*, 462(7274):778–781.

Garcia-Castellanos, D. and Villaseñor, A. (2011). Messinian salinity crisis regulated by competing tectonics and erosion at the gibraltar arc. *Nature*, 480(7377):359–363.

Gargani, J. and Rigollet, C. (2007). Mediterranean sea level variations during the messinian salinity crisis. *Geophysical Research Letters*, 34(10).

Giosan, L., Filip, F., and Constatinescu, S. (2009). Was the black sea catastrophically flooded in the early holocene? *Quaternary Science Reviews*, 28(1-2):1–6.

Gladstone, R., Flecker, R., Valdes, P., Lunt, D., and Markwick, P. (2007). The mediterranean hydrologic budget from a late miocene global climate simulation. *Palaeogeography, Palaeoclimatology, Palaeoecology*, 251(2):254–267.

Goldberg, S. L., Lau, H. C., Mitrovica, J. X., and Latychev, K. (2016). The timing of the black sea flood event: Insights from modeling of glacial isostatic adjustment. *Earth and Planetary Science Letters*, 452:178–184.

Govers, R. (2009). Choking the mediterranean to dehydration: the messinian salinity crisis. *Geology*, 37(2):167–170.

Govers, R., Meijer, P., and Krijgsman, W. (2009). Regional isostatic response to messinian salinity crisis events. *Tectonophysics*, 463(1-4):109–129.

Gupta, S., Collier, J. S., Palmer-Felgate, A., and Potter, G. (2007). Catastrophic flooding origin of shelf valley systems in the english channel. *Nature*, 448(7151):342–345.

Han, D., Wahr, J., Cohen, S., and Vanicek, P. (1989). Post-glacial rebound analysis for a rotating earth. *Slow Deformations and Transmission of Stress in the Earth*, 49:1–6.

Hiscott, R., Aksu, A., Yaşar, D., Kaminski, M., Mudie, P., Kostylev, V., MacDonald, J., Işler, F., and

Lord, A. (2002). Deltas south of the bosphorus strait record persistent black sea outflow to the marmara sea since 10 ka. *Marine Geology*, 190(1-2):95–118.

Johnston, P. (1993). The effect of spatially non-uniform water loads on prediction of sea-level change. *Geophysical Journal International*, 114(3):615–634.

Kendall, R. A., Mitrovica, J. X., and Milne, G. A. (2005). On post-glacial sea level–ii. numerical formulation and comparative results on spherically symmetric models. *Geophysical Journal International*, 161(3):679–706.

Krijgsman, W., Fortuin, A., Hilgen, F., and Sierro, F. J. (2001). Astrochronology for the messinian sorbas basin (se spain) and orbital (precessional) forcing for evaporite cyclicity. *Sedimentary Geology*, 140(1-2):43–60.

Krijgsman, W., Hilgen, F., Raffi, I., Sierro, F. J., and Wilson, D. (1999). Chronology, causes and progression of the messinian salinity crisis. *Nature*, 400(6745):652–655.

Lambeck, K. (1996). Shoreline reconstructions for the persian gulf since the last glacial maximum. *Earth and Planetary Science Letters*, 142(1-2):43–57.

Lambeck, K. and Nakada, M. (1990). Late pleistocene and holocene sea-level change along the australian coast. *Palaeogeography, Palaeoclimatology, Palaeoecology*, 89(1-2):143–176.

Lambeck, K., Purcell, A., and Zhao, S. (2017). The north american late wisconsin ice sheet and mantle viscosity from glacial rebound analyses. *Quaternary Science Reviews*, 158:172–210.

Lambeck, K., Sivan, D., and Purcell, A. (2007). Timing of the last mediterranean sea black sea connection from isostatic models and regional sea-level data. In *The Black Sea Flood Question: Changes in Coastline, Climate, and Human Settlement*, pages 797–808. Springer.

Latychev, K., Mitrovica, J. X., Tromp, J., Tamisiea, M. E., Komatitsch, D., and Christara, C. C. (2005). Glacial isostatic adjustment on 3-d earth models: a finite-volume formulation. *Geophysical Journal International*, 161(2):421–444.

Lericolais, G., Guichard, F., Morigi, C., Minereau, A., Popescu, I., and Radan, S. (2010). A post younger dryas black sea regression identified from sequence stratigraphy correlated to core analysis and dating. *Quaternary International*, 225(2):199–209.

Lugli, S., Manzi, V., Roveri, M., and Schreiber, C. B. (2010). The primary lower gypsum in the mediterranean: A new facies interpretation for the first stage of the messinian salinity crisis. *Palaeogeography, Palaeoclimatology, Palaeoecology*, 297(1):83–99.

Major, C., Ryan, W., Lericolais, G., and Hajdas, I. (2002). Constraints on black sea outflow to the sea of marmara during the last glacial–interglacial transition. *Marine Geology*, 190(1-2):19–34.

Milne, G. A. and Mitrovica, J. X. (1996). Postglacial sea-level change on a rotating earth: first results from a gravitationally self-consistent sea-level equation. *Geophysical Journal International*,

126(3):F13–F20.

Milne, G. A. and Mitrovica, J. X. (1998). Postglacial sea-level change on a rotating earth. *Geophysical Journal International*, 133(1):1–19.

Milne, G. A., Mitrovica, J. X., and Davis, J. L. (1999). Near-field hydro-isostasy: the implementation of a revised sea-level equation. *Geophysical Journal International*, 139(2):464–482.

Mitrovica, J. X. and Milne, G. A. (2003). On post-glacial sea level: I. general theory. *Geophysical Journal International*, 154(2):253–267.

Mitrovica, J. X. and Peltier, W. R. (1991). On postglacial geoid subsidence over the equatorial oceans. *Journal of Geophysical Research: Solid Earth*, 96(B12):20053–20071.

Mitrovica, J. X., Wahr, J., Matsuyama, I., and Paulson, A. (2005). The rotational stability of an ice-age earth. *Geophysical Journal International*, 161(2):491–506.

Nicholas, W. A., Chivas, A. R., Murray-Wallace, C. V., and Fink, D. (2011). Prompt transgression and gradual salinisation of the black sea during the early holocene constrained by amino acid racemization and radiocarbon dating. *Quaternary Science Reviews*, 30(27-28):3769–3790.

Ohneiser, C., Florindo, F., Stocchi, P., Roberts, A. P., DeConto, R. M., and Pollard, D. (2015). Antarctic glacio-eustatic contributions to late miocene mediterranean desiccation and reflooding. *Nature communications*, 6(1):1–10.

Peltier, W. (1974). The impulse response of a maxwell earth. *Reviews of Geophysics*, 12(4):649–669.

Peltier, W. (1998). Postglacial variations in the level of the sea: Implications for climate dynamics and solid-earth geophysics. *Reviews of Geophysics*, 36(4):603–689.

Peltier, W. and Drummond, R. (2002). A broad-shelf effect upon postglacial relative sea level history. *Geophysical research letters*, 29(8):10–1.

Peltier, W. R. and Andrews, J. T. (1976). Glacial-isostatic adjustmenti. the forward problem. *Geophysical Journal International*, 46(3):605–646.

Peltier, W. R., Argus, D., and Drummond, R. (2015). Space geodesy constrains ice age terminal deglaciation: The global ice-6g_c (vm5a) model. *Journal of Geophysical Research: Solid Earth*, 120(1):450–487.

Periáñez, R. and Abril, J. (2015). Computational fluid dynamics simulations of the zanclean catastrophic flood of the mediterranean (5.33 ma). *Palaeogeography, Palaeoclimatology, Palaeoecology*, 424:49–60.

Rohling, E., Schiebel, R., and Siddall, M. (2008). Controls on messinian lower evaporite cycles in the mediterranean. *Earth and Planetary Science Letters*, 275(1-2):165–171.

Roveri, M., Flecker, R., Krijgsman, W., Lofi, J., Lugli, S., Manzi, V., Sierro, F. J., Bertini, A., Camerlenghi, A., De Lange, G., et al. (2014). The messinian salinity crisis: past and future of a great

challenge for marine sciences. *Marine Geology*, 352:25–58.

Ryan, W. B., Major, C. O., Lericolais, G., and Goldstein, S. L. (2003). Catastrophic flooding of the black sea. *Annual Review of Earth and Planetary Sciences*, 31(1):525–554.

Ryan, W. B., Pitman III, W. C., Major, C. O., Shimkus, K., Moskalenko, V., Jones, G. A., Dimitrov, P., Gorür, N., Sakinç, M., and Yüce, H. (1997). An abrupt drowning of the black sea shelf. *Marine geology*, 138(1-2):119–126.

Soulet, G., Ménot, G., Lericolais, G., and Bard, E. (2011). A revised calendar age for the last reconnection of the black sea to the global ocean. *Quaternary Science Reviews*, 30(9-10):1019–1026.

Teller, J. T., Glennie, K. W., Lancaster, N., and Singhvi, A. K. (2000). Calcareous dunes of the united arab emirates and noah's flood: the postglacial reflooding of the persian (arabian) gulf. *Quaternary International*, 68:297–308.

Woodward, R. S. (1888). *On the Form and Position of the Sea Level: With Special References to Its Dependence on Superficial Masses Symmetrically Disposed about a Normal to the Earth's Surface*. Number 48. US Government Printing Office.

Wu, P. and Peltier, W. (1984). Pleistocene deglaciation and the earth's rotation: a new analysis. *Geophysical Journal International*, 76(3):753–791.

Wu, P. and van der Wal, W. (2003). Postglacial sealevels on a spherical, self-gravitating viscoelastic earth: effects of lateral viscosity variations in the upper mantle on the inference of viscosity contrasts in the lower mantle. *Earth and Planetary Science Letters*, 211(1-2):57–68.

Yanko-Hombach, V., Mudie, P. J., Kadurin, S., and Larchenkov, E. (2014). Holocene marine transgression in the black sea: New evidence from the northwestern black sea shelf. *Quaternary International*, 345:100–118.

Zhong, S., Paulson, A., and Wahr, J. (2003). Three-dimensional finite-element modelling of earths viscoelastic deformation: effects of lateral variations in lithospheric thickness. *Geophysical Journal International*, 155(2):679–695.

APPENDIX A: IMPLEMENTATION INCLUDING SHORELINE MIGRATION

In the following, we generalize the treatment in the main text to present 'sea-level equations' incorporating shoreline migration for both the case of one water body and two isolated water bodies. For the sake of brevity, in the following equations the dependence of various fields on colatitude and east longitude is implicit. We also use a subscript j to denote the time $t = t_j$ or the j^{th} time step ending at $t = t_j$.

A1 One Water Body

The sea-level equation valid for a single water body (i.e., global ocean) and time varying shoreline geometry was presented by Mitrovica and Milne (2003). Their expressions involved changes in sea level from the beginning of the simulation. However, as discussed in the main text, it is desirable in the present application to express all equations in terms of the change across a single time step. In this case, we derive the following, exact expression for the change in ocean height,

$$\delta S_j = \delta S L_j C_j - T_{j-1}[C_j - C_{j-1}]. \tag{A.1}$$

Combining this expression with Equation 17 yields

$$\delta S_j = \left[\delta \mathcal{SL}_j + \frac{\delta \Phi_j}{g}\right] C_j - T_{j-1}[C_j - C_{j-1}]. \tag{A.2}$$

The j^{th} increment to the uniform shift in the height of the sea-surface equipotential can be computed by invoking conservation of mass. Integrating both sides of equation A.2 over the surface of the Earth, gives

$$\frac{\delta \Phi_j}{g} = \frac{1}{A_j}\iint_\Omega \delta S_j \mathrm{d}\Omega - \frac{1}{A_j}\iint_\Omega \delta \mathcal{SL}_j C_j \mathrm{d}\Omega + \frac{1}{A_j}\iint_\Omega T_{j-1}[C_j - C_{j-1}]\mathrm{d}\Omega \tag{A.3}$$

where

$$A_j = \iint_\Omega C_j \mathrm{d}\Omega. \tag{A.4}$$

Conservation of mass requires that

$$\iint_\Omega \delta S_j \mathrm{d}\Omega = -\frac{\rho_i}{\rho_w}\iint_\Omega \delta I_j \mathrm{d}\Omega, \tag{A.5}$$

and combining this with Equation A.3 yields

$$\frac{\delta \Phi_j}{g} = -\frac{1}{A_j}\frac{\rho_i}{\rho_w}\iint_\Omega \delta I_j \mathrm{d}\Omega - \frac{1}{A_j}\iint_\Omega \delta \mathcal{SL}_j C_j \mathrm{d}\Omega + \frac{1}{A_j}\iint_\Omega T_{j-1}[C_j - C_{j-1}]\mathrm{d}\Omega. \tag{A.6}$$

Equations (A.2), (A.4) and (A.6) represent the sea-level equation for the single water body case allowing for shoreline migration.

A2 Two Isolated Water Bodies: Ocean & Lake

Expressions analogous to Equations (A.2), (A.4) and (A.6) for the two water body system are as follows. For the open ocean:

$$\delta S_{o,j} = \left[\delta\mathcal{SL}_j + \frac{\delta\Phi_{o,j}}{g}\right] C_{o,j} - T_{j-1}[C_{o,j} - C_{o,j-1}] \tag{A.7}$$

$$\begin{aligned}\frac{\delta\Phi_{o,j}}{g} = &-\frac{1}{A_{o,j}}\frac{\rho_i}{\rho_w}\iint_\Omega \delta I_j \mathrm{d}\Omega + \frac{\delta E(t_j)}{A_o} - \frac{1}{A_{o,j}}\iint_\Omega \delta\mathcal{SL}_j C_{o,j}\mathrm{d}\Omega \\ &+ \frac{1}{A_{o,j}}\iint_\Omega T_{j-1}[C_{o,j} - C_{o,j-1}]\mathrm{d}\Omega\end{aligned} \tag{A.8}$$

where

$$A_{o,j} = \iint_\Omega C_{o,j}\mathrm{d}\Omega. \tag{A.9}$$

For the lake:

$$\delta S_{m,j} = \left[\delta\mathcal{SL}_j + \frac{\delta\Phi_{m,j}}{g}\right] C_{m,j} - T_{j-1}[C_{m,j} - C_{m,j-1}] \tag{A.10}$$

$$\frac{\delta\Phi_{m,j}}{g} = -\frac{\delta E(t_j)}{A_{m,j}} - \frac{1}{A_{m,j}}\iint_\Omega \delta\mathcal{SL}_j C_{m,j}\mathrm{d}\Omega + \frac{1}{A_{m,j}}\iint_\Omega T_{j-1}[C_{m,j} - C_{m,j-1}]\mathrm{d}\Omega \tag{A.11}$$

where

$$A_{m,j} = \iint_\Omega C_{m,j}\mathrm{d}\Omega. \tag{A.12}$$

As in Section 2.2, all melt water from ice sheets enters the open ocean, rather than the lake, and evaporative flux acts to remove water from the lake an add it to the open ocean.

Finally, the combined incremental ocean height change for the whole Earth is calculated as the sum of that for the open ocean and for the lake, to solve for the change in sea level.

$$\delta S_j = \delta S_{o,j} + \delta S_{m,j} \tag{A.13}$$

APPENDIX B: TRANSITIONS

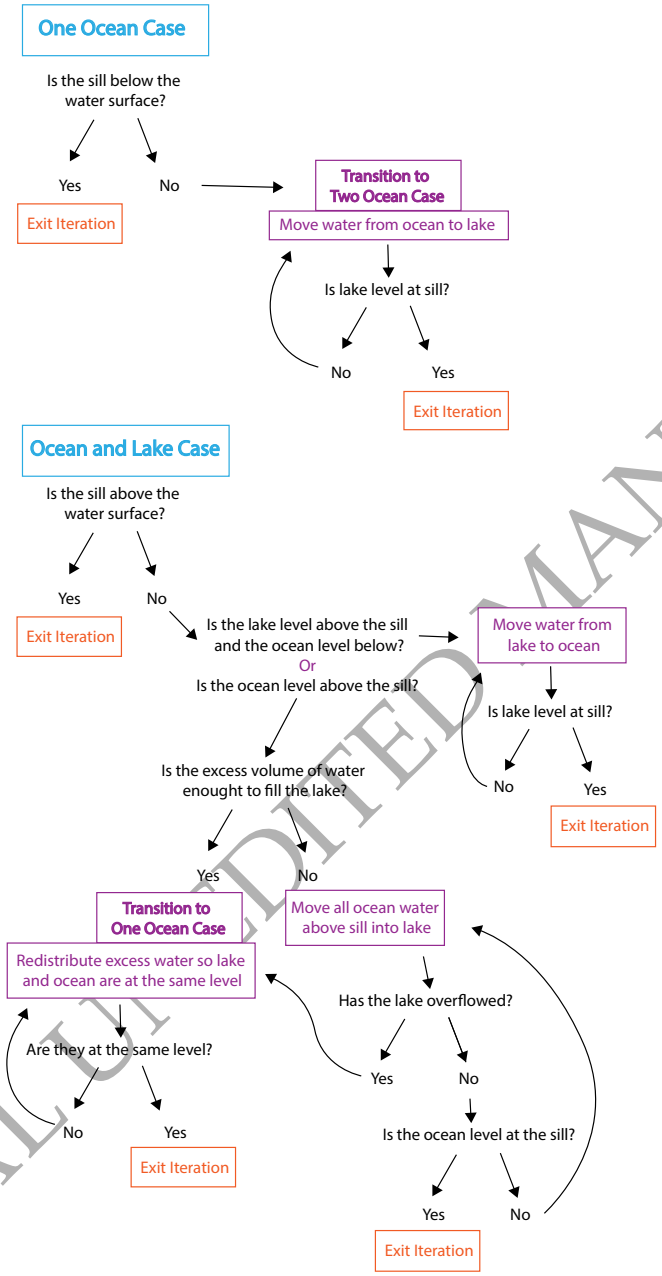

Figure B.1. Flowchart giving qualitative description of transitional phases. The two primary cases, described in the main text in Sections 2.1 and 2.2 are given in blue. The main transitions, described in Sections 2.3.1 and 2.3.2 are given in bold purple.

APPENDIX C: COMPARISON TO APPROXIMATE TREATMENTS

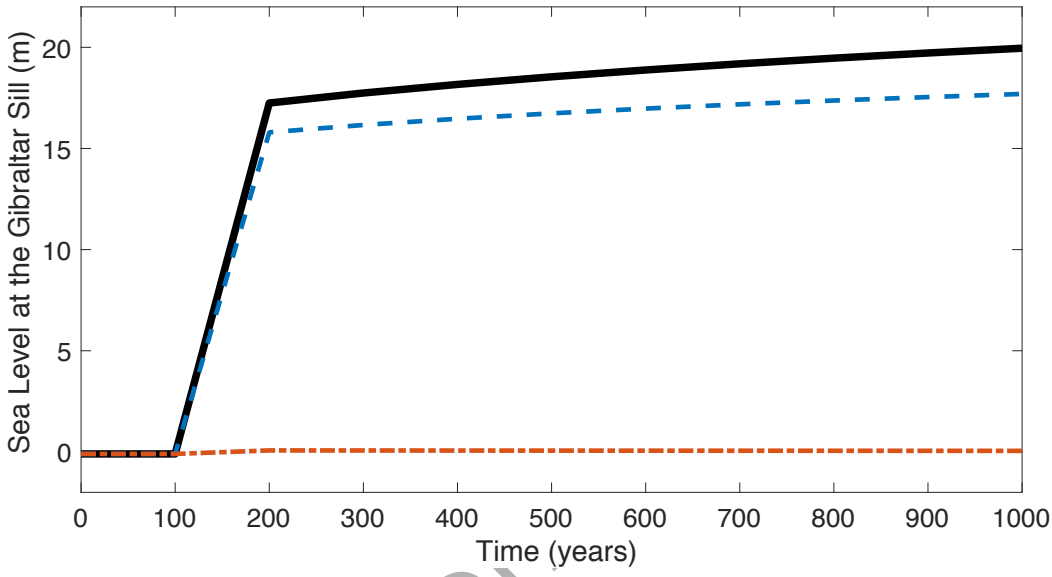

Figure C.1. Evolution of sea level at the Gibraltar Sill generated following a breach of the sill specifically, a scenario in which ice melt into the global ocean elevates local sea level to 5 cm above the Gibraltar sill (before water is allowed to enter the Mediterranean). The solid black line shows the sea-level rise predicted by the extended sea-level theory. In this case, the initial flux of water in the Mediterranean leads to a positive feedback (see Section 4 of the main text) that fills the Mediterranean ocean basin. The dashed lines give results based on two approximate treatments of flooding which require that the flood volume and geometry be prescribed *a-priori*. The first calculation (red dash-dot line) assumes a uniform filling that follows the geometry of the initial Mediterranean topography, with a volume equal to the excess volume overtopping the sill in the global ocean. This assumption follows the approach of Coulson et al. (2019) and it involves no additional flooding of the Mediterranean beyond the initial prescribed volume, and no redistribution of flood water within the Mediterranean. In the second treatment (blue dashed line), the prescribed flood is given by the volume and geometry defined by the initial empty Mediterranean topography. Once again, no additional flooding or flood water redistribution occurs within the Mediterranean.